

Islet Amyloid Polypeptide: Identification of Long-range Contacts and Local Order on the Fibrillogenesis Pathway

Shae B. Padrick and Andrew D. Miranker*

Department of Molecular
Biophysics and Biochemistry
Yale University, 266 Whitney
Avenue, PO Box 208114, New
Haven, CT 06520, USA

The pathology of type II diabetes includes deposition of amyloid in the extra cellular space surrounding the β -cells of the endocrine pancreas. The principle component of these deposits is an insoluble fibrillar form of a normally soluble 37 residue peptide hormone, islet amyloid polypeptide. Multiple sequence analysis and peptide synthesis have identified a core set of residues (20 to 29) as intrinsically amyloidogenic. As the fibrillogenesis of the 20-29 peptide often requires conditions that deviate considerably from physiological, residues 20 to 29 may be necessary, but not sufficient, for amyloidosis. We aim to determine the structural role of residues outside this core in the context of *in vitro* fibrillogenesis of the wild-type peptide at physiological pH and ionic strength. Specifically, we make use of an intrinsic fluorescent probe, tyrosine 37 (Y37), to explore the role of the C terminus in fibrillogenesis. Our protocol permits steady state measurement of the lag phase and fiber conformational states of the protein under identical conditions. These are compared to a non-amyloidogenic variant of islet amyloid polypeptide from rat and *N*-acetyl-tyrosinamide as models of the unfolded state under matched conditions. Spectral, quenching and anisotropic properties of Y37 in the fiber state indicate that the C terminus is packed in a well-defined environment with near frozen rigidity. The presence of a fluorescence resonance energy transfer pathway shows Y37 is near F15 and F23. The lag-phase conformation, while considerably less ordered than the fiber, is more ordered than unfolded models. Differences in anisotropy between the lag and fiber state were used to monitor fibrillogenesis in real time. Parallel assessment of fiber formation using the histological dye, ThT, indicate that ordering at the C terminus of islet amyloid polypeptide is coincident with, and thus indicative of, fiber formation.

© 2001 Academic Press

*Corresponding author

Keywords: IAPP; tyrosine fluorescence; type II diabetes; amyloid; amylin

Introduction

The deposition of normally soluble protein as amyloid fiber is central to a number of diseases including, for example, Alzheimer's and dialysis

related amyloidosis.¹ This problem is particularly fascinating as proteins that are apparently unrelated in sequence and in their native conformations nevertheless aggregate into fibrils with common structural and histological features.² These features include a crossed- β sheet organization in which the β -strands are arranged perpendicular to the fibril axis, and the display of green birefringence upon binding of the dye Congo Red. Amyloid fiber formation kinetics also share common features.³ Fibrillogenesis reactions are characterized by a lag phase during which no fibers are observed. This is then followed by a period of fiber formation on a timescale that can be shorter than the lag phase. Furthermore, the lag phase can often be bypassed by nucleating a reaction with preformed fibers.

Abbreviations used: FRET, fluorescence resonance energy transfer; IAPP, islet amyloid polypeptide; hIAPP, human IAPP; hIAPP_{lag}, the lag phase conformation of hIAPP; hIAPP_{fib}, the fibrillar conformation of hIAPP; rIAPP, rat IAPP; HFIP, 1,1,1,3,3,3-hexafluoroisopropanol; NAYA, *N*-acetyl tyrosinamide; nMAC, *N*-methyl acetamide; ThT, Thioflavin T.

E-mail address of the corresponding author:
Andrew.Miranker@yale.edu

Greater than 90% of type II diabetics have amyloid deposits surrounding the islet cells of the pancreas.⁴ These deposits are predominantly made of fibers composed of islet amyloid polypeptide (IAPP). IAPP is a 37-residue peptide which is co-secreted with insulin by the β cells. A number of possible metabolic roles have been suggested for IAPP, e.g. slowing of pyloric emptying into the duodenum⁵ and attenuation of insulin secretion by β cells.⁶ Increased insulin secretion (and therefore IAPP secretion) is the normal response to insulin resistance in type II diabetics. As IAPP fibers have been shown to be toxic to cultured β cells,⁷ the development of IAPP fibers is thought to amplify the diabetic state through severe depletion in the number of β cells available to secrete insulin.

The covalent structure of IAPP in diabetics is identical to that found in healthy individuals. Furthermore, *in vitro* fiber formation occurs at IAPP concentrations below the concentration found in the secretory granule (ca 400 μ M).⁸⁻¹⁰ This implies that a change in the environment of IAPP is responsible for the conformational change to insoluble amyloid fiber in diabetics. Subsets of the IAPP sequence, e.g. 20-29¹¹ and 30-37¹² have been characterized and shown to form fibers. Independent fiber formation by these peptides suggests that they may be in a similar conformation to that seen for the same stretch of amino acid residues in the full-length fiber. We note, however, that the concentrations required for fiber formation by these sequences are often orders of magnitude higher than that required for the full-length peptide. This suggests that additional interactions are necessary for the formation and stability of wild-type IAPP fibers.

Here, we have used the intrinsic aromatic residues of IAPP to study conformational change induced by fibrillogenesis of the full-length peptide. As wild-type IAPP possesses a single tyrosine and no tryptophans (Figure 1), we are able to make several specific and complementary studies of this residue. Excitation and emission profiles, steady state anisotropy, quenching behavior and resonant energy transfer between internal aromatics are all used to develop a structural description of IAPP prior to and after fibrillogenesis.

Results

Polymerization time for human IAPP (hIAPP) is strongly dependent on reaction conditions and procedures for preparation of stock solutions.¹³ For this work, we chose a single reaction condition that

reproducibly generates a lag phase in excess of ten minutes with fibrillogenesis complete in less than 1 hr (Figure 2). We refer to the conformational ensemble of hIAPP before fibrillogenesis as hIAPP- P_{lag} and after fibrillogenesis as hIAPP- P_{fib} . Our time-scale is determined from the midpoint, $t_{1/2}$, for maximal fluorescence enhancement of the histological dye, Thioflavin T (ThT)¹⁴ (Figure 2). The reaction (initiated by a 1:40 dilution of a 1 mM stock solution of hIAPP in HFIP, with 100 mM KCl, 50 mM potassium phosphate (pH 7.4) at 25 °C) yields a final protein concentration of 25 μ M. This readily permits steady state intrinsic fluorescence measurements to be conducted before and after the transition. There are three fluorescent residues in hIAPP: F15, F23 and Y37 (Figure 1). The maximum absorbance of tyrosine is $\epsilon_{275} = 1.4 \times 10^3 \text{ M}^{-1} \text{ cm}^{-1}$ while that of phenylalanine is $\epsilon_{255} = 0.22 \times 10^3 \text{ M}^{-1} \text{ cm}^{-1}$.¹⁵ Furthermore, the quantum yield of fluorescence for tyrosine is approximately fourfold higher than for phenylalanine. We can assume, therefore, that light detected upon excitation at 278 nm is entirely derived from Y37.

Two reference molecules are used to evaluate hIAPP- P_{lag} and hIAPP- P_{fib} under matched solution conditions. As a baseline for interpretation of fluorescence, we use a tyrosine analogue. Our choice, *N*-acetyl-tyrosinamide (NAYA), reflects the presence of C-terminal amidation in IAPP. As a model of the unfolded state, we use a sequence variant of IAPP from rat (rIAPP) (Figure 1). The relevance of rIAPP to these studies is derived from two observations. First, the far UV CD spectrum of rIAPP under our reaction conditions is characteristic of a random coil (data not shown).¹³ Second, although rIAPP is 84% identical to hIAPP, it is non-amyloidogenic. This has been attributed to the presence of three proline residues, which are known to be strong β -sheet breakers.¹⁶ These two reference molecules permit changes in the spectral properties of rIAPP versus hIAPP- P_{lag} and hIAPP- P_{lag} versus hIAPP- P_{fib} to be interpreted in terms of unfolded to lag-phase and lag-phase to fiber structural transitions, respectively.

Electronic environment of Y37

The excitation maximum for NAYA under our reaction conditions is 275 nm (Figure 3(a)), excitation of which yields an emission profile with a maximum at 300 nm (Figure 3(b)). At wavelengths that are longer than their peak maxima, the excitation profile of NAYA, rIAPP, hIAPP- P_{lag} are nearly

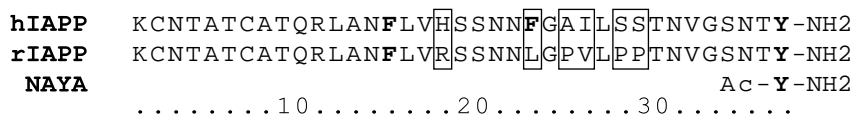


Figure 1. Amino acid sequence of hIAPP, rIAPP, and NAYA. NAYA is shown here schematically. Changes between hIAPP and rIAPP sequences are in boxes. Intrinsic fluorescent aromatic residues are highlighted in bold.

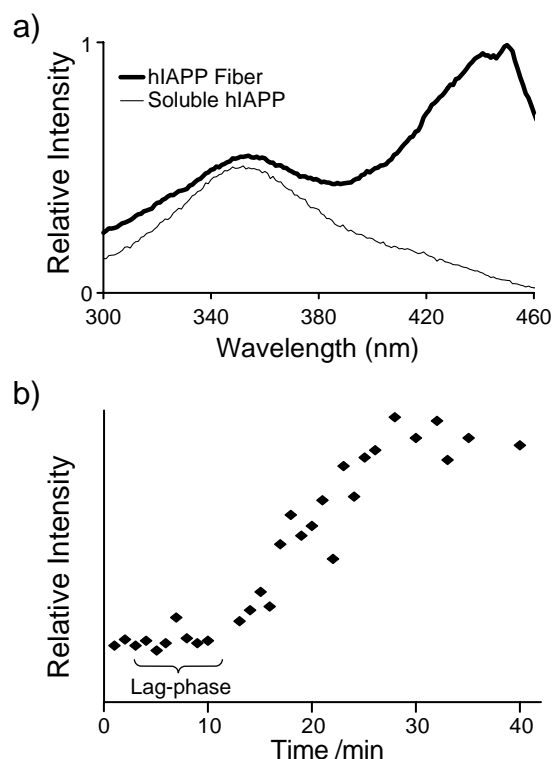


Figure 2. Fiber formation kinetics followed by ThT fluorescence. (a) Fluorescence of ThT is enhanced upon binding fiber. hIAPP as preformed fibers (thick line), or monomer stock solution in HFIP (thin line) was diluted to identical concentration (in monomer units) with ThT containing buffer. For fibers, the fluorescence excitation spectrum between 430 and 460 nm is dramatically increased. Emission is detected at 482 nm. (b) Kinetics followed by ThT fluorescence. Aliquots of a standard fiber formation reaction are removed at successive time points and quenched by dilution with ThT assay buffer. Excitation intensities are integrated from 430–460 nm.

identical (Figure 3(a)). By contrast, the relative intensity of excitation transitions at these longer wavelengths is greater for hIAPP_{fib}. An increase in relative intensity at wavelengths near 287 nm has also been observed in absorbance and fluorescence excitation measurements of the interaction of free tyrosine with peptide backbone mimics, such as *N*-methyl acetamide (nMAC).^{17,18} These investigations have suggested that these lower energy transitions are enhanced when the tyrosine hydroxyl oxygen accepts a hydrogen bond. We made an analogous study under our reaction conditions by determining the difference spectrum of NAYA in the presence and absence of 1 M nMAC (Figure 3(c)). Comparing this to the difference spectrum of NAYA and hIAPP_{fib} clearly shows similarities at wavelengths above 275 nm.

Excitation profiles at wavelengths that are shorter than 265 nm show a clear progression in the fluorescent intensity of rIAPP, hIAPP_{lag} and hIAPP_{fib} compared to NAYA (Figure 3(a)). This is most

readily seen at 250 nm. As this is 24.5 nm below the excitation maximum for NAYA and as the slope of the excitation of NAYA at 250 nm can be seen approaching 0, it seems unlikely that intensity at this wavelength is the result of direct excitation of tyrosine. One possibility is that this trend is the result of excitation of phenylalanine. As we collect emission 25 nm above the emission λ_{\max} phenylalanine and, since the quantum yield for phenylalanine is 1/4 that of tyrosine, our observations would reflect fluorescence resonance energy transfer (FRET), not direct emission of phenylalanine. This can occur with measurable efficiency, for example in histone-like protein from *Thermoplasma acidophilum*,¹⁹ provided the distance between donor (F) and acceptor (Y) is less than 18 Å (efficiency = 10 %).

To confirm that our observation is due to FRET, we first compared the difference spectrum of hIAPP_{fib} and NAYA with the excitation spectrum of free phenylalanine (Figure 3(c)). A correspondence can clearly be seen at wavelengths below 270 nm. Second, we were able to monitor the quenching of the phenylalanine fluorescence by the presence of the acceptor, tyrosine (Figure 3(d)). By monitoring emission at 278 nm rather than 303 nm, we ensured that fluorescence of phenylalanine would predominate over that of tyrosine. The excitation spectrum of hIAPP_{lag} clearly shows a maximum at 258 nm indicating that some direct emission of phenylalanine fluorescence can still be measured from this conformational state. Upon fiber formation, a distinct peak for phenylalanine fluorescence is no longer observed. This indicates complete quenching of the fluorescence of both phenylalanine residues.

Emission profiles of rIAPP and hIAPP_{lag} are indistinguishable from NAYA (Figure 3(b)), although intensities are diminished by ~80 % (Figure 3(b), inset). This loss of intensity between free tyrosine and tyrosine incorporated in peptides is well known and largely attributed to quenching by the carbonyl group of peptide bonds.^{17,20} By contrast, the emission profile of hIAPP_{fib} differs markedly from NAYA. A substantially greater proportion of hIAPP_{fib} emission is at wavelengths that are shorter than the maximum (300 nm). While this is due in part to a small increase in the direct scatter intensity brought about by the presence of fibers, scatter cannot account for the diminishment of intensity above 300 nm. Blue shifts in tryptophan fluorescence are commonly attributed to burial of the indole moiety in the hydrophobic core of a protein. This does not follow for tyrosine as its emission is far less sensitive to environment. Emission λ_{\max} of phenol derivatives such as NAYA, for example, is unchanged in solvents as diverse as water and 1,4-dioxane.¹⁷

Solvent accessibility of the C terminus

The excited state of tyrosine, as any fluorophore, returns to the ground state via a number of path-

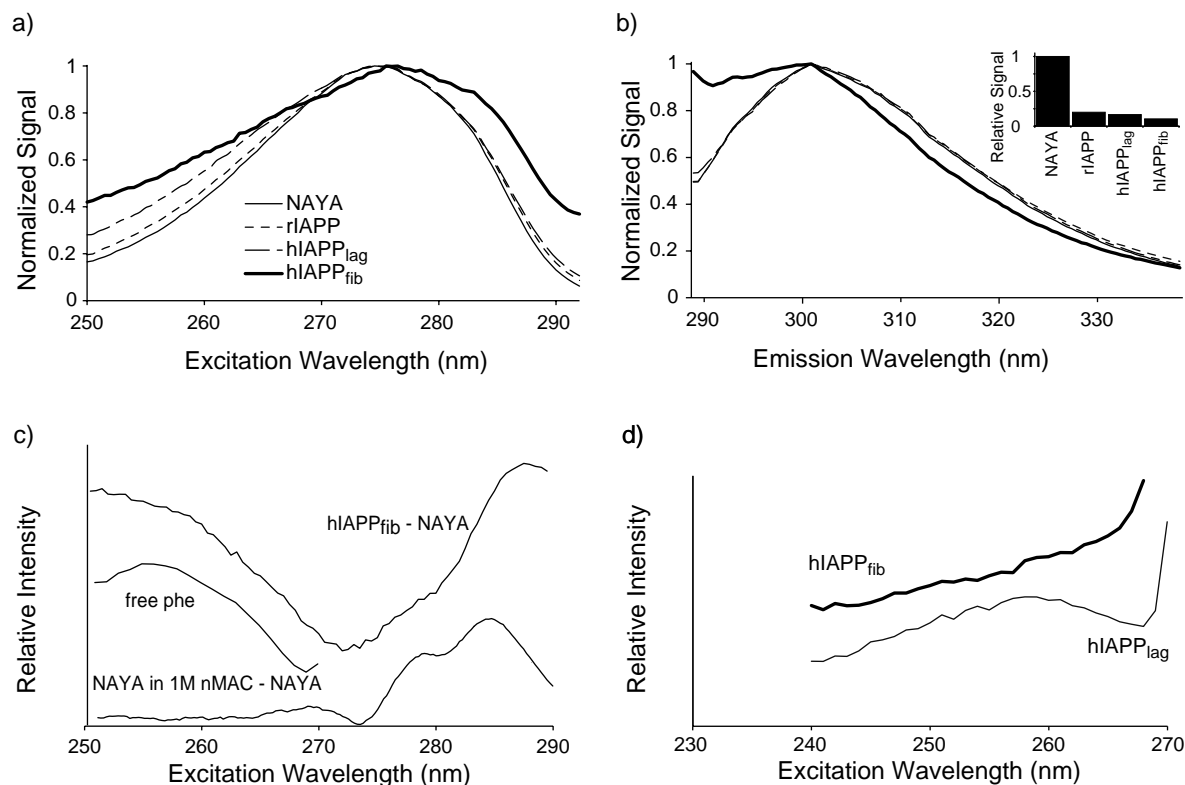


Figure 3. Intrinsic fluorescence of IAPP. (a) Normalized fluorescence excitation spectra for NAYA, rIAPP, hIAPP_{lag} and hIAPP_{fib}. All spectra acquired under identical conditions. Emission is observed at 303 nm. (b) Normalized fluorescence emission spectra for NAYA, rIAPP, hIAPP_{lag} and hIAPP_{fib}. All spectra acquired under identical conditions. Excitation wavelength is 278 nm. Curve identities are shown in (a). The spectra for NAYA, rIAPP and hIAPP_{lag} overlap. (Inset) Relative fluorescent intensity for samples in (a) and (b). Intensities measured at excitation wavelength 275 nm and emission wavelength 300 nm. IAPP concentrations were 25 μ M in all samples. NAYA concentration 5 μ M and scaled by 5. (c) Difference spectrum of hIAPP_{fib} and NAYA shown in (a). Two distinct peaks are observed, one with a λ_{max} above 278 nm, the other below. An excitation spectrum of 500 μ M free phenylalanine is shown (emission observed at 278 nm), and corresponds to the blue shifted peak of hIAPP_{fib}-NAYA. The difference spectrum of [NAYA in 1 M nMAC]-[NAYA in H₂O] and corresponds to the red shifted peak of hIAPP_{fib}-NAYA. Curves have been offset for clarity. Latter curve was smoothed using a 2 nm rolling average. (d) Fluorescence excitation spectrum of hIAPP, detecting at 278 nm. A peak for phenylalanine is readily apparent in hIAPP_{lag} and absent in hIAPP_{fib}.

ways, of which, only one is emission of a photon detectable as fluorescence. The proportion of molecules that emit a photon can be greatly diminished by addition of a soluble quenching agent to the solution. Quenching is dependent, in part, on contact of the quenching agent with the fluorophore. This provides an effective means of characterizing the local environment of a fluorophore in terms of solvent accessibility, e.g. Garzon-Rodriguez *et al.*²¹ We have made use of this to study the conformation of IAPP in terms of the solvent accessibility of Y37.

The effect of the quenching agent, acrylamide, was determined for NAYA, rIAPP, hIAPP_{lag} and hIAPP_{fib} over a quenching agent concentration range of 0 to 100 mM (Figure 4(a)). As expected, NAYA is most easily quenched with 60% of the fluorescence intensity lost at 100 mM acrylamide. By comparison, the extent to which rIAPP is

quenched by 100 mM acrylamide is smaller. The difference between rIAPP and NAYA most likely stems from the slower diffusion of rIAPP. Quenching of Y37 in hIAPP_{lag} shows a further reduction over rIAPP. While the difference is small, it is consistent and is also qualitatively observed when I⁻ is used as the quenching agent. The difference between rIAPP and hIAPP_{lag} is most readily explained by a conformational difference between the two that either affords a greater degree of solvent protection for Y37 in hIAPP_{lag} or a significantly larger hydrodynamic radius for hIAPP_{lag}.

Conversion of hIAPP_{lag} to a fibrillar state results in a dramatic reduction in the sensitivity of Y37 to quenching. At 100 mM acrylamide, fluorescence in hIAPP_{fib} is reduced by only 39% compared to 51% in hIAPP_{lag}. A reduction in quenching may result from either solvent exclusion, or a reduced diffusion rate. Collisional quenching is, however,

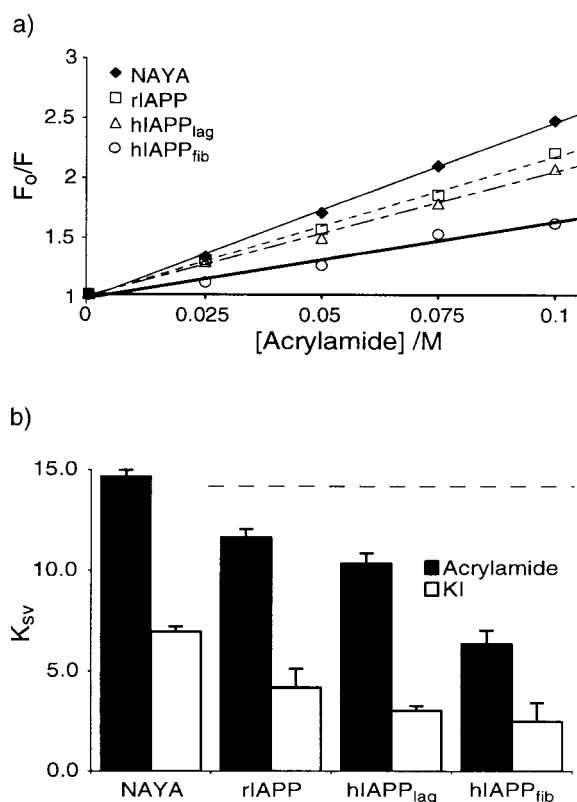


Figure 4. Measurement of solvent accessibility by quenching of intrinsic fluorescence. (a) Stern-Volmer analysis of quenching of IAPP fluorescence by acrylamide. Data was fit to the equation $F_0/F = K_{SV}[Q] + b$, where F is the fluorescence intensity at concentration $[Q]$ of quencher. For clarity, points shown are averages of three measurements, although statistics were determined using all points. All lines extrapolate back to $b = 1(\pm 0.03)$ at $[Q] = 0$ M. Pearson's R for fits of acrylamide quenching are 0.997, 0.994, 0.985, and 0.944 for NAYA, rIAPP, hIAPP_{lag} and hIAPP_{fib}, respectively. (b) Values of K_{SV} for quenching of tyrosine fluorescence by acrylamide (filled bars) or iodide (open bars). Heavy line at $K_{SV} = 14.2$ M⁻¹ represents a theoretical estimate of acrylamide quenching (see Materials and Methods) for a 100% solvent exposed tyrosine in monomeric IAPP being quenched by acrylamide. Error bars are the standard error in the slope of the fit.

proportional to the sum of the fluorophore and quencher diffusion rates.¹⁵ As the diffusion rate for both hIAPP_{lag} and hIAPP_{fib} is small in comparison to that of acrylamide, diminished sensitivity of hIAPP_{fib} to quenching reflects burial of Y37.

Quenching can arise from either binding of quenching agent, or diffusion controlled collisions. Furthermore, multiple protein conformations may contribute to the observed quenching behavior. To address these issues, fluorescence in the absence of quenching agent (F_0) and as a function of quenching agent concentration (F) was measured. Plots of F_0/F as a function of acrylamide concentration (Stern-Volmer analysis) show linear behavior.

Furthermore, the fits consistently extrapolate to an intercept of $1(\pm 0.03)$ (Figure 4(a)). This strongly suggests that only single conformers are contributing to our observations. The slopes of the fits, K_{SV} , describe the ease of quenching in a physically interpretable way. Our measurements were repeated using I^- as the quenching agent (Figure 4(b)). The trends observed for acrylamide and I^- are similar, although the absolute magnitudes are not. The reduced degree by which I^- quenches compared to acrylamide likely reflects its reduced quenching efficiency. The similarity of the behavior of the two quenching agents suggests that the quenching of Y37 in IAPP is the result of diffusion-controlled collisions of quenching agent with phenol groups that are in structurally homogeneous environments.

An independent approach to measuring solvent accessibility is the measurement of the pK_a of the tyrosine. If buried or partially buried, tyrosine will ionize at an increased pK_a .²² Tyrosinate, tyrosine's conjugate base, has dramatically less fluorescent intensity at 303 nm. Therefore, we can measure the pK_a of tyrosine by monitoring the loss of fluorescent intensity as a function of pH (Figure 5). We presumed that hIAPP_{lag} would be affected by pH and therefore measured the pK_a of tyrosine in NAYA, rIAPP and hIAPP_{fib} only. Subsequent ThT analysis of hIAPP_{fib} samples incubated at these pH values showed a <10% variation in fiber content. NAYA exhibits a pK_a of 9.9, which is a commonly observed value for tyrosine pK_a . Titration of rIAPP yields data within error to that of NAYA (data now shown). hIAPP_{fib} however shows a pK_a which is increased by nearly two full pK_a units, to a pK_a of 11.8. We attribute this shift to partial hydrophobic burial of Y37.

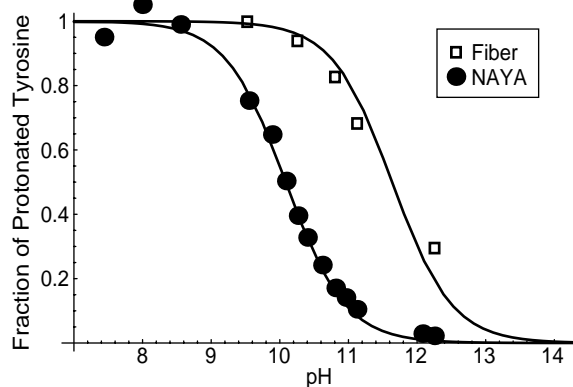


Figure 5. Titration of Y37 in hIAPP_{fib}. Titration of 5 μ M of hIAPP_{fib} is observed by quenching of Y37 fluorescence intensity. Lower baseline for both NAYA and hIAPP_{fib} correspond to zero intensity. hIAPP_{fib} did not dissolve at high pH, as measured by ThT. 5 μ M samples of NAYA show 50% titration at pH 9.9, consistent with literature values. Curves are plots of the Henderson-Hasselbalch equation for a single ionizing species, using pK_a 's of 9.9 and 11.8, respectively.

Rotational freedom of Y37

Anisotropy of fluorescence emission, r , is dependent on the ability of a fluorophore to rotate during the lifetime of its excited state. Rotational freedom can therefore be related to the size and rigidity of the atoms surrounding the fluorophore. As conversion of precursor to amyloid fiber is necessarily accompanied by an increase in molecular weight, steady state anisotropy was measured (Figure 6). A clear and consistent progression of increasing anisotropy was observed with $\text{NAYA} < \text{rIAPP} < \text{hIAPP}_{\text{lag}} < \text{hIAPP}_{\text{fib}}$.

We assume that the development of anisotropy is the result of rigid, spherically shaped packing of protein atoms around the tyrosine side-chain. We further assume that the fluorescent lifetime of tyrosine, τ_0 , does not change in the three states of IAPP. The fundamental, or maximal, anisotropy for NAYA, $r_0 = 0.278$ ($\lambda_{\text{ex}} = 280$ nm), is determined from the anisotropy of NAYA in frozen solution.²³ Within these caveats, the rotational correlation time, θ , can be extracted using the Perrin equation, ($r^{-1} = r_0^{-1} + \tau_0/(r_0\theta)$), and the relative molecular volumes, which are proportional to θ are 1:2:4:100 for NAYA, rIAPP, hIAPP_{lag} and hIAPP_{fib} respectively (Figure 6). As many assumptions are required for this assessment, it is impossible to conclude more than that there is a progressive increase of conformational order near the phenol group in NAYA, rIAPP, and hIAPP_{lag}. The transition of hIAPP_{lag} to hIAPP_{fib} however results in a dramatic change. Indeed, the anisotropy for hIAPP_{fib} is nearly the same as NAYA in frozen solution. This strongly suggests that the increase of anisotropy is the result of oligomeric assembly.

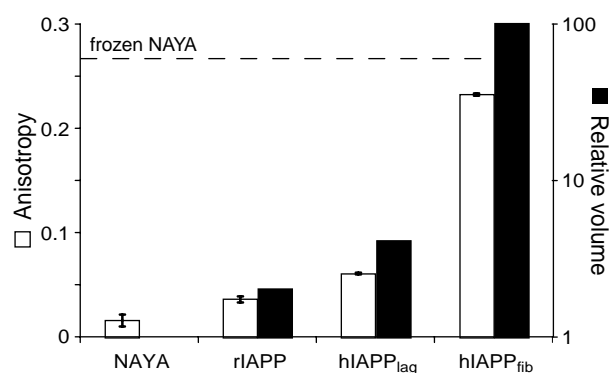


Figure 6. Steady state anisotropy of Y37. Anisotropy of NAYA, rIAPP, hIAPP_{lag} and hIAPP_{fib} are shown with open bars. Dashed line is the value observed for the anisotropy of NAYA in frozen solution.²³ Relative volume (filled bars) is calculated for a spherical fluorophore whose rotational diffusion describes the observed anisotropy. Averages of three measurements are shown, error bars are $\pm 1\text{SD}$. Note, error shown for hIAPP_{fib} is ± 0.001 . However, we observe anisotropy to be dependent on reaction conditions with values ranging from 0.22 to 0.26.

The increase in fluorescence anisotropy from rIAPP to hIAPP_{lag} can be explained by an increase in local order and/or by an oligomeric complex. The latter can be tested for using static light scatter. Detecting light scatter at 340 nm (Figure 7) we observe that scatter by rIAPP is marginal. By contrast, hIAPP_{fib} produces considerable scatter, presumably as fiber length is well in excess of 340 nm. It is surprising that hIAPP_{lag} also produces scatter intensity within a factor of two of that seen for hIAPP_{fib}. This is consistent with hIAPP_{lag} containing large oligomeric complexes.

Simultaneous collection of perpendicular and parallel emission permits measurement of the anisotropy in real time (Figure 8). This approach generates a lag phase with $t_{1/2} = 16(\pm 3)$ minutes and elongation time constant of $180(\pm 50)$ seconds. This is consistent with our kinetics measured by mass spectrometry under similar conditions.²⁴ Furthermore, fiber formation kinetics of hIAPP²⁵ can be measured indirectly using the histological dye, ThT.¹⁴ Changes in the fluorescence intensity of the dye are directly proportional to the quantity of fiber in the sample. We conducted this measurement in parallel with the measurement of anisotropy. As aliquots of the reaction are quenched by dilution into assay buffer containing ThT, they can be assayed after anisotropy data collection is complete. The profile of the increase in ThT fluorescence clearly parallels the transition measured by anisotropy (Figure 8). This demonstrates that the formation of a rigid environment around tyrosine 37 is coincident with ThT detectable fiber formation.

The standard deviations of our measurements of anisotropy for NAYA, rIAPP and hIAPP_{lag} are small (< 0.01). This is also true for hIAPP_{fib} (SD 0.001), however, in reactions under similar but not identical solution conditions (data not shown), hIAPP_{fib} anisotropy values range from 0.22 to 0.26.

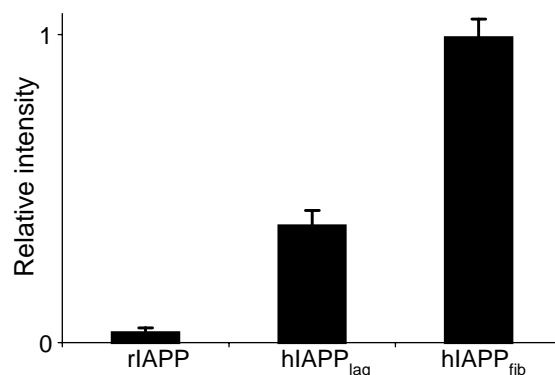


Figure 7. Static light scatter of rIAPP, hIAPP_{lag} and hIAPP_{fib}. 90° static light scatter is observed from objects with a dimension on the order of or greater than the wavelength of light used for measurement (340 nm). Reported values are the average of three independent measurements with buffer contribution subtracted. Error bars are $\pm 1\text{SD}$.

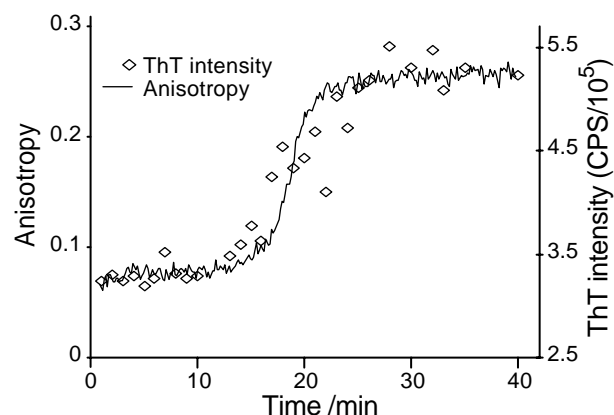


Figure 8. Fiber formation kinetics of hIAPP followed by Y37 fluorescence anisotropy. A single fiber formation reaction is initiated and split into two aliquots. Half is used for real-time anisotropy measurements, the remainder for ThT assays. Overlay of ThT dye-binding assay intensity and tyrosine anisotropy show close agreement of the midpoints of the fiber formation transition. Real time anisotropy measurements made with one second averaging, nine second delay between points to minimize photobleaching.

Sensitivity of apparent anisotropy to the exact composition of the fibril mixture is likely to contribute to this variability. Using negative stain transmission electron microscopy, our fiber preparations appear to be formed from 5 nm-wide protofibers which have assembled into a range of higher order fiber morphologies (data not shown). This is consistent with previously reported data in which 5 nm protofibers are also seen to assemble into several well-characterized morphologies, e.g. 8 nm and 11 nm forms.²⁶ A second source of variability may arise from the contribution of 1–2 μM of precursor which remains after fibrillogenesis is apparently complete.²⁴

Discussion

The structural determinants of amyloid formation are challenging to characterize since fiber preparations are intrinsically heterogeneous in both length and width. The intermediates of fiber formation exist transiently allowing only limited time for study. The experiments performed here have nevertheless allowed us to elucidate several aspects of the structure of both the lag-phase and fiber conformations of IAPP.

The observation that intrinsic fluorescence in NAYA, rIAPP and hIAPP_{lag} is more readily quenched than in hIAPP_{fib} (Figure 4) can be explained by a significant change in exposed surface area. We estimate this change by comparing hIAPP_{fib} with rIAPP. The predicted K_{SV} for tyrosine in rIAPP in an extended conformation is 14.2 M^{-1} (see Materials and Methods). As our measurement, 11.7 M^{-1} , is similar, we take this lat-

ter value to represent 100% exposure to solvent. The K_{SV} measured for hIAPP_{fib} ($K_{SV} = 6.4 \text{ M}^{-1}$) therefore reflects a solvent exposure of 55%. This may reflect partial burial of all fluorophores, or complete burial of a fraction of the fluorophores. The latter is improbable given the apparent absence of curvature in the Stern-Volmer plots (Figure 4(a)). As a complementary approach to assess the existence of two or more fiber populations with distinct solvent accessibilities, we monitored quenching of tyrosine fluorescence by deprotonation. Our titration curve for NAYA yields a pK_a of 9.9 while that of hIAPP_{fib} is 11.8 (Figure 5). A shift of ~ 2 units is consistent with partial burial and is comparable to pK_a shifts seen in folded proteins, e.g. thermolysin.²² Furthermore, as the pK_a could be determined using a single site model and since deprotonation results in a complete loss of fluorescence intensity, it is unlikely that our measurement of solvent exposure reflects a weighted average of exposed and occluded populations. This is particularly important, as the fiber preparation contains a mixture of fiber morphologies.²⁶ Our observation of linear quenching behavior and single component ionization indicates either that a single local conformation is present under our conditions or that all conformations have similar solvent exposure for their C termini.

The maximum possible value for fluorescence anisotropy is 0.4,²⁷ which can occur provided the fluorophore is rigidly oriented during the excited state lifetime, it does not interact with its environment and the absorption and emission moments are parallel. For real samples, a limiting anisotropy, r_0 , can be determined by making measurements in a vitreous environment (e.g. frozen to -62°C , in 70% (v/v) propylene glycol). For our model compound, NAYA, this yields $r_0 = 0.278$, while for proteins and peptides, values range from 0.21 (histone H1) to 0.28 (leu5-enkephalin).²³ At 25°C in an aqueous environment, we measure the steady state anisotropy of hIAPP_{fib} to be 0.235. This implies that the conformational flexibility of Y37 in hIAPP_{fib} is comparable to proteins in frozen solution. Specifically, Y37 does not rotate on a timescale shorter than the lifetime of the excited state (1–3ns).

For heterogeneous fibers, this is not necessarily the expected result. Fibers formed from SH3 domains, for example, have helical repeat lengths that vary within a given fiber.²⁸ One interpretation of this is that fibers are fluid at a local level. Given the loss of entropy upon fiber formation, this could be an effective means of recapturing some of this loss. By contrast, well-defined internuclear distances and unusually narrow linewidths have been determined for fibers formed from peptide fragments of A β using solid state NMR methods.^{29,30} These measurements are consistent with homogeneous, crystal-like rigidity. Thus, the side-chain of Y37 in hIAPP_{fib} behaves much like the residues of fibrillar A β . This is surprising given that Y37 is

eight residues outside the proposed amyloidogenic core.

Upon conversion of hIAPP_{lag} to hIAPP_{fib}, the emission λ_{\max} is unchanged (Figure 3(b)). However, a change in the profile shifts the first moment (intensity weighted wavelength average) by 2 nm to shorter wavelengths. This is unusual as it is more typical that tyrosine quantum yield, but not emission profile are affected by protein conformation or solution conditions. Our observation can be explained either by the existence of a novel excited state complex, or by the excited state complex forming contacts and sampling vibrations which are similar to the ground state complex. The latter would result in changes to the excitation spectrum as well as the emission spectrum.¹⁵ We favor the latter explanation since it correlates with the appearance of enhanced excitation in hIAPP_{fib} at 285 nm. As this absorbance mode corresponds to transitions in the phenol ring that are not associated with molecular vibration,^{18,31} our conjecture is consistent with our observations of anisotropy. Namely that Y37 in hIAPP_{fib} exists in an environment which is rigid both with respect to stretching vibrations as well as free space and side-chain rotations.

The presence of resonant energy transfer from F15 and/or F23 to Y37 requires that these residues be near in space. Transfer efficiency between phenylalanine and tyrosine in hIAPP_{fib} was estimated to be 84% by the enhanced fluorescence of Y37 (see Materials and Methods). FRET efficiency in excess of 50% requires that both F15 and F23 be near in space to Y37. Donor quenching was not used for this calculation as phenylalanine emission was too weak to be used reliably. Assuming both phenylalanines are equidistant from Y37, a transfer efficiency of 84% corresponds to a distance of 10.2 Å. Alternatively, assuming one phenylalanine is very close to Y37 (efficiency = 100%), the furthest the other phenylalanine can be from Y37 is 11 Å.

These distances permit us to limit the possible models of fiber structure. For example, the C α -to-C α intramolecular distance separating F23 and Y37 while in an extended β conformation is 48 Å. F to Y FRET cannot be reliably observed for distances greater than 18 Å, as efficiency is less than 10%. It is clear that this is not the source of energy transfer. Contact is therefore the result of either intramolecular proximity mediated by a turn between Y37 and F23 or intermolecular contact between adjacent strands, or both. In the case of turn-free β -strands, it is difficult to reconcile the FRET data. For example, an in register parallel β -sheet, such as that proposed for fibrillar A β ₁₀₋₃₅,³⁰ would generate interstrand distances greater than the intrastrand distances described above. In addition, as 10.2 Å is consistent with measured intersheet packing distances in amyloid fibers,² it is also possible that energy transfer takes place between two stacked β -sheets in the fiber. As with adjacent strands, strands on adjacent sheets cannot be in register, as

they would generate F15/23 to Y37 distances in excess of those determined by FRET measurement. A protofibrillar width of 5 nm corresponds to a maximum β -strand length of about 15 residues, assuming a cross β model. Therefore, the IAPP fiber must either include turns, or else the majority of IAPP residues must be unstructured and outside the fiber core. The measurement of FRET from F15 to Y37 suggests that the former is true. Assuming the presence of turns and antiparallel packing, F to Y FRET in hIAPP_{fib} can therefore be accommodated by models in which transfer is either wholly intramolecular, or else intermolecular involving two or three polypeptides.

hIAPP fibers generated *in vitro* contain a mixture of morphologies derived from assembly of 5 nm protofibrils (data not shown).²⁶ This suggests that there could be two or more distinct environments for Y37. Our results, however, suggest that the environment of Y37 is homogeneous and well defined. Quenching analysis and pK_a determinations are both sensitive to contributions from multiple species, yet both are consistent with a single contributor. In a similar way, if a significantly populated conformer contained a fully exposed and therefore mobile phenol ring, we would not expect the measured anisotropy of 0.235 to have approached the limiting value of 0.278. Finally, a homogeneous environment is also suggested by the near maximal transfer efficiency of fluorescence energy from a phenylalanine residue to tyrosine. The presence of a significant population of conformers in which phenylalanine and tyrosine are far apart would have given rise to a reduced transfer efficiency. This suggests that despite morphological differences all the fibers have a similar underlying local environment near Y37.

For hIAPP_{lag}, the behavior of Y37 was expected to be similar to that of rIAPP. Both have predominantly random coil secondary structure as determined by far UV CD,^{13,32} and both have similar (84% identical) primary sequence. Indeed, residues 30 to 37 are identical (Figure 1). The behavior of hIAPP_{lag} however, consistently differs from that of rIAPP. Quenching behavior (Figure 4) shows that Y37 is somewhat more protected from solvent exposure in hIAPP_{lag} ($K_{SV,acrylamide} = 10.4 \text{ M}^{-1}$) than in rIAPP ($K_{SV,acrylamide} = 11.7 \text{ M}^{-1}$). Interpreted in terms of a change in surface area, this corresponds to an 11% loss of exposed surface area. As quenching of hIAPP and rIAPP are dominated by the diffusion of quenching agents not by motion of the monomers, changes in diffusion of the peptides are unlikely to explain this observation. Rather, a conformational or oligomeric change that alters solvent exposure of Y37 must be invoked. The anisotropy of hIAPP_{lag} is consistently 0.025(±0.005) greater than rIAPP. This can be explained either by a reduction in the rotational mobility of Y37, or a shortening of the fluorescence lifetime in hIAPP_{lag}. Both of these possibilities

require a similar conformational or oligomeric difference between rIAPP and hIAPP_{lag}.

Phenylalanine to tyrosine FRET is also evident in hIAPP_{lag} (Figure 3(a)). FRET efficiency is 31 % for rIAPP and 48 % for hIAPP_{lag}; these efficiencies correspond to phenylalanine to tyrosine distances of 14.3 Å and 12.6 Å, respectively. A random walk model³³ of the polypeptide backbone predicts the average distance between residues Y37/F23 and Y37/F15 to be 30 Å and 40 Å, respectively. At this distance, FRET transfer efficiencies are <1 %. It is clear that the phenylalanine and tyrosine residues are much closer in space than expected for an unfolded protein. Taken together, anisotropy, quenching and FRET suggest that rIAPP and hIAPP_{lag} are collapsed into compact structures. rIAPP and hIAPP_{lag} both show evidence of little secondary structure (data not shown and refs. 13,32). Light scattering experiments (Figure 7) can distinguish between monomeric and multimeric models of rIAPP and hIAPP_{lag}. Light scatter from rIAPP is measurably greater than, but of the same order as, background. This implies a monomer or low order oligomer. hIAPP_{lag} shows a large quantity of scattered light, about half that seen for the fibers. The furthest possible C^α to C^α distance between terminal residues is in an extended β-sheet conformation, which for a 37 residue peptide is 12 nm. As this is well below the wavelength of light used in these scattering experiments (340 nm), hIAPP_{lag} must be an oligomer. It is important to consider oligomeric interactions during the lag phase, for example, micellar interactions have been proposed for Aβ^{34,35} and hIAPP_{20-29,T30W}.³⁶ Further structural characterization of the hIAPP_{lag} conformation is thus of great interest as oligomeric states and residual structure may have a role in fibrillogenesis.

A number of fragments of hIAPP have been observed to form fibers: hIAPP₂₀₋₂₉,^{11,16,37,38} hIAPP₂₀₋₂₇, hIAPP₂₂₋₂₇, hIAPP₂₃₋₂₇,³⁸ hIAPP₁₇₋₃₇, hIAPP₂₄₋₃₇, hIAPP₂₄₋₂₉, hIAPP_{Ac24-29}, hIAPP₃₀₋₃₇, hIAPP_{Ac30-37},¹² proline residues containing mutants of hIAPP₂₀₋₂₉ S20P, N21P, S29P, A25P¹⁶ and hIAPP₂₀₋₃₀ T30W.³⁶ Full-length, wild-type hIAPP can form fibers in less than one hour at 25 μM in pH 7.4 buffer, at an ionic strength near that of serum. Fiber formation by fragments of hIAPP is typically achieved over a period of days, with millimolar concentrations of peptide, extreme pH, solvent or temperature conditions, or a mixture of these. For example, hIAPP₂₀₋₂₉ forms fibers at 10 mg/ml in 10 % (v/v) acetic acid¹¹ and hIAPP₂₂₋₂₇ and hIAPP₂₃₋₂₇ forms fibers at 5 mM but neutral pH.³⁸

It has recently been suggested that fiber formation is a generic property of all proteins provided suitable conditions are found.³⁹ Proteins whose amyloidogenic conditions happen to be close to physiological give rise to clinical disorders. A corollary to this hypothesis is that any peptide fragment from any protein is also capable of forming fibers. This statement has an interesting conse-

quence. Namely, that the identification of an amyloidogenic peptide from a full-length amyloidogenic protein does not necessarily indicate that the peptide participates in fibril formation by the intact protein. It is important, therefore to complement fragment analysis with full-length studies.

Our work complements the results of fragment analysis by providing a clear picture of the role of the C terminus in the full-length hIAPP fiber. Residues 30 to 37, synthesized as a fragment, are amyloidogenic.¹² However, residues 30 to 37 are not amyloidogenic in the context of rIAPP's primary sequence. Our work shows that in order to form mature hIAPP fibers, structures must be formed which include contacts between Y37, F15 and F23. Long-range interactions are therefore critical to the fiber formation kinetics and subsequent stability of mature hIAPP fibers.

Materials and Methods

Materials

hIAPP was synthesized in house by standard t-Boc solid-phase methods and purified by reverse phase HPLC. Synthetic rIAPP was obtained from BAChem. ThT was purchased from Acros. HFIP was acquired from Sigma-Aldrich and further purified by fractional distillation (59-60 °C). NAYA, nMAC and phenylalanine were acquired from Sigma-Aldrich. Buffers and salts were purchased from J.T. Baker with three exceptions, CAPS buffer was acquired from Sigma-Aldrich, TrisHCl, glycine, and acrylamide were acquired from American Bioanalytical.

Preparation of samples

To remove trace quantities of preformed fiber which can seed fiber formation, hIAPP stocks were prepared in 7 M guanidine HCl and bound to a C18 reverse phase micro tip column (AmiKa), washed, and eluted with 100 % HFIP. We have observed that hIAPP fibers are retained on C18 resin, even in the presence of a high percentage organic solvent. Stocks were kept at 4 °C. The concentration of peptide stock solutions was calculated using absorption at 280 nm, using a calculated extinction coefficient^{40,41} of 1400 M⁻¹ cm⁻¹. hIAPP stock concentration was 0.75 mM. A 1 mM stock solution of rat IAPP was prepared directly from a lyophilized powder by addition of water.

Standard solution conditions for all experiments were 25 μM of IAPP, 3 % (v/v) HFIP, 100 mM KCl, 50 mM potassium phosphate (pH 7.4). To account for a difference in quantum yields, NAYA samples use 5 μM NAYA as standard concentration. Data reported for hIAPP_{lag} were collected between three to eight minutes after sample preparation. After every analysis, 8 μl of sample was assayed for ThT binding. Data points were discarded if ThT binding indicated ≥10 % conversion to fiber.

Fiber suspensions were made by preparing 100 μl of 50 μM hIAPP, 6 % HFIP, 100 mM KCl, 50 mM potassium phosphate (pH 7.4), and incubating for ten minutes at 21-23 °C, then diluting to standard conditions.

Fluorescence

All fluorescence experiments were performed on a PTI C-61 T-form fluorescence spectrophotometer fitted with a temperature controlled cell holder. Glan-Thompson style plane polarizers were used in anisotropy experiments. Slit widths were 5 nm in all cases. All fluorescence spectra were measured in a 3 mm × 3 mm Hellma fluorescence cuvette with 200 μ l sample volume. Tyrosine excitation scans were performed by scanning excitation wavelengths from 260 nm to 293 nm, 1 nm steps, emission wavelength set to 303 nm. Tyrosine emission scans were performed with the excitation wavelength set to 278 nm, emission wavelength varied from 288 nm to 340 nm, in 1 nm steps. Spectra shown in Figure 3(a) and (b) and those used for calculating the spectra in Figure 3(c) are normalized to their maximum intensity. Spectra were corrected for variations in lamp intensity, detector and monochromator wavelength dependent sensitivity, except for Figure 3(d) as correction factors were unavailable below 240 nm. Anisotropy and quenching measurements were excited at 278 nm and emission was observed at 303 nm. G-factor corrections were applied to the anisotropy data. Quenching information was obtained by preparing identical concentrations of IAPP or NAYA in standard conditions with the addition of acrylamide or substitution of KI for KCl. Tyrosine spectra, anisotropy and quenching values were measured in triplicate.

Presence or absence of amyloid fibers was demonstrated using a ThT binding assay.¹⁴ Lag-phase hIAPP containing solutions were diluted to 1.0 μ M hIAPP in 200 μ l of 5 μ M ThT, 50 mM glycine buffer (pH 9). Fiber samples, pH samples and kinetic time points were diluted to 0.5 μ M hIAPP. Quantitative measures were made by integrating excitation wavelengths 430 nm–460 nm.

pH titration

A pH titration of Y37 in hIAPP_{fib} was performed by dilution of fibers into buffers of several pH values. Fibers were made at 50 μ M hIAPP, 6% HFIP, in 100 mM KCl, 1 mM phosphate buffer (pH 7.4). After ten minutes of incubation at 21–23 °C, the solution was found to contain fibers by ThT and the fibers were diluted 1:10 to a final concentration of 5 μ M, 100 mM KCl, and 50 mM of buffer. Buffers used were: Tris (pH 8.0), Tris (pH 8.5), glycine (pH 9.4), glycine (pH 9.6), glycine (pH 9.8), glycine (pH 10.0), CAPS (pH 10.2), CAPS (pH 10.4), CAPS (pH 10.6), CAPS (pH 10.8), CAPS (pH 11.0), phosphate (pH 12.0), phosphate (pH 12.5). After 15 minutes, emission spectra of the samples were taken, excitation wavelength 278 nm, emission wavelength 290 nm through 340 nm.

Light scatter

Light scatter measurements were made using the spectrofluorometer described above, fitted with Glan-Thompson polarizers, in parallel orientation. Slit widths were 3 nm. Intensities were corrected for lamp fluctuations. Excitation and emission wavelengths were set to 340 nm. Signal was collected over 60 seconds. Measurements were repeated three times, with background subtraction.

Calculations

FRET efficiency was calculated using as adaptation of the enhanced acceptor fluorescence method described by Lakowicz.¹⁵ The fluorescence observed at 303 nm when excited at 256 nm may be described as proportional to the sum of light absorbed directly by tyrosine plus light absorbed by phenylalanine and transferred with efficiency, E , to tyrosine. Assuming fluorescence upon excitation at 278 nm is dominated by tyrosine and phenylalanine does not emit appreciably at 303 nm:

$$E = \frac{F_{\text{Sample}}^N - F_{\text{NAYA}}^N}{A_{\text{Mix}}^N - F_{\text{NAYA}}^N} \quad (1)$$

Where $F^N(x)$ is the fluorescence of the sample, x , when excited at 256 nm, emission observed at 303 nm and normalized to the emission intensity when excited at 275 nm. $A^N(\text{mix})$ is the absorbance at 256 nm, normalized by the absorbance at 275 nm. (mix) is either a 2:1 or 1:1 mixture of phenylalanine:NAYA for use with hIAPP or rIAPP, respectively.

The donor-acceptor distance, R , was calculated from E using:

$$E = \frac{R_0^6}{R_0^6 + R^6} \quad (2)$$

Where R_0 is the critical distance. We used a value of 12.5 Å for R_0 , which is the average of the two reported values of R_0 for phenylalanine to tyrosine transfer.^{19,42}

Random walk distances were calculated using Flory's random walk model.^{33,43} F15 \rightarrow Y37 (hIAPP) C $^\alpha$ -C $^\alpha$ distance was calculated using a 20-alanine and two-glycine model. F23 \rightarrow Y37 (hIAPP) C $^\alpha$ -C $^\alpha$ distance was calculated using a 12-alanine and two-glycine model. F15 \rightarrow Y37 (rIAPP) C $^\alpha$ -C $^\alpha$ distance was calculated using a 17-alanine, two-glycine and three-proline model.

For diffusion controlled quenching, Stern-Volmer constants may be related to diffusion rates by:

$$\frac{K_{SV}}{\tau_0} = \alpha f_Q k_0 \approx \frac{\alpha 4\pi N_A}{1000} (R_c)(D_f + D_q) \quad (3)$$

Where τ_0 is the lifetime, R_c is the contact distance for the fluorophore and quenching agent, D_f is the diffusion constant of the fluorophore, D_q is the diffusion constant of the quenching agent, N_A is Avogadro's number. f_Q is the quenching efficiency, which is near 1 for acrylamide and iodide.¹⁵ α is the fraction of solvent exposed surface area. We assume τ_0 to be constant and 3 ns. Contact distance, R_c , is estimated to be 6 Å. Diffusion constants were estimated using the Stokes-Einstein equation. Molecular radius for monomeric IAPP is estimated to be 11 Å, the radius of a sphere at density 0.72 g/ml and molecular weight of 3900 Da. Radius of acrylamide is 2.8 Å. Solution viscosity is estimated by the viscosity of water. If we assume for rIAPP, hIAPP_{lag} and hIAPP_{fib}, contact distance is unchanged, $D_q \gg D_f$ and τ_0 is unchanged, then the relative solvent exposure, α , can be estimated from the ratio of K_{SV} s.

Midpoint of the kinetic transition (Figure 8) is found by fitting the data to a sigmoid with independent, linear baselines before and after the transition. Elongation kinetics measured by fitting the last 40% of the transition to a single exponential. All exponential and sigmoid fits performed using the NonlinearRegress function in the NonlinearFit package of Mathematica 3.0.⁴⁴

Acknowledgments

We thank Drs C.J. Morgan, G. Sarkis, M. Ramirez-Alvarado and G. Olack for helpful discussions and critical reading of this manuscript. This work supported by the National Institutes of Health (DK54899). S.P. is supported by a National Science Foundation Graduate Research Fellowship. A.D.M. is a Pew Scholar in the biomedical sciences.

References

- Rochet, J. C. & Lansbury, P. T., Jr (2000). Amyloid fibrillogenesis: themes and variations. *Curr. Opin. Struct. Biol.* **10**, 60-68.
- Sunde, M., Serpell, L. C., Bartlam, M., Fraser, P. E., Pepys, M. B. & Blake, C. C. (1997). Common core structure of amyloid fibrils by synchrotron X-ray diffraction. *J. Mol. Biol.* **273**, 729-739.
- Harper, J. D. & Lansbury, P. T., Jr (1997). Models of amyloid seeding in Alzheimer's disease and scrapie: mechanistic truths and physiological consequences of the time-dependent solubility of amyloid proteins. *Annu. Rev. Biochem.* **66**, 385-407.
- Kahn, S. E., Andrikopoulos, S. & Verchere, C. B. (1999). Islet amyloid: a long-recognized but underappreciated pathological feature of type 2 diabetes. *Diabetes*, **48**, 241-253.
- Young, A. A., Gedulin, B., Vine, W., Percy, A. & Rink, T. J. (1995). Gastric emptying is accelerated in diabetic BB rats and is slowed by subcutaneous injections of amylin. *Diabetologia*, **38**, 642-648.
- Gebre-Medhin, S., Olofsson, C. & Mulder, H. (2000). Islet amyloid polypeptide in the islets of Langerhans: friend or foe? *Diabetologia*, **43**, 687-695.
- Lorenzo, A., Razzaboni, B., Weir, G. C. & Yankner, B. A. (1994). Pancreatic-islet cell toxicity of amylin associated with type-2 diabetes-mellitus. *Nature*, **368**, 756-760.
- Hutton, J. C. (1989). The insulin secretory granule. *Diabetologia*, **32**, 271-281.
- Kahn, S. E., D'Alessio, D. A., Schwartz, M. W., Fujimoto, W. Y., Ensink, J. W. & Taborsky, G. J., Jr *et al.* (1990). Evidence of cosecretion of islet amyloid polypeptide and insulin by β -cells. *Diabetes*, **39**, 634-638.
- Westermarck, P., Li, Z. C., Westermarck, G. T., Leckstrom, A. & Steiner, D. F. (1996). Effects of beta cell granule components on human islet amyloid polypeptide fibril formation. *FEBS Lett*, **379**, 203-206.
- Westermarck, P., Engstrom, U., Johnson, K. H., Westermarck, G. T. & Betsholtz, C. (1990). Islet amyloid polypeptide: pinpointing amino acid residues linked to amyloid fibril formation. *Proc. Natl Acad. Sci. USA*, **87**, 5036-5040.
- Nilsson, M. R. & Raleigh, D. P. (1999). Analysis of amylin cleavage products provides new insights into the amyloidogenic region of human amylin. *J. Mol. Biol.* **294**, 1375-1385.
- Higham, C. E., Jaikaran, E. T., Fraser, P. E., Gross, M. & Clark, A. (2000). Preparation of synthetic human islet amyloid polypeptide (IAPP) in a stable conformation to enable study of conversion to amyloid-like fibrils. *FEBS Letters*, **470**, 55-60.
- LeVine, H. D. (1993). Thioflavine T interaction with synthetic Alzheimer's disease β -amyloid peptides: detection of amyloid aggregation in solution. *Protein Sci.* **2**, 404-410.
- Lakowicz, J. R. (1999). *Principles of Fluorescence Spectroscopy*, Kluwer Academic/Plenum Publishers, New York.
- Moriarty, D. F. & Raleigh, D. P. (1999). Effects of sequential proline substitutions on amyloid formation by human amylin₂₀₋₂₉. *Biochemistry*, **38**, 1811-1818.
- Ross, R. T. & Lee, J. (1998). Absorption and fluorescence of tyrosine hydrogen-bonded to amide-like ligands. *J. Phys. Chem. B*, **102**, 4612-4618.
- Strickland, E. H., Wilchek, M., Horwitz, J. & Billups, C. (1972). Effects of hydrogen bonding and temperature upon the near ultraviolet circular dichroism and absorption spectra of tyrosine and O-methyl tyrosine derivatives. *J. Biol. Chem.* **247**, 572-580.
- Searcy, D. G., Montenay-Garestier, T. & Helene, C. (1989). Phenylalanine-to-tyrosine singlet energy transfer in the archaeobacterial histone-like protein HTa. *Biochemistry*, **28**, 9058-9065.
- Creed, D. (1984). The photophysics and photochemistry of the near-UV absorbing amino acids-II. Tyrosine and its simple derivatives. *Photochem. Photobiol.* **39**, 563-575.
- Garzon-Rodriguez, W., Vega, A., Sepulveda-Becerra, M., Milton, S., Johnson, D. A. & Yatsimirsky, A. K., *et al.* (2000). A conformation change in the carboxyl-terminus of Alzheimer's A β ₁₋₄₀ accompanies the transition from dimer to fibril as revealed by fluorescence quenching analysis. *J. Biol. Chem.* **275**, 22645-22649.
- Lee, S. B., Inouye, K. & Tonomura, B. (1997). The states of tyrosyl residues in thermolysin as examined by nitration and pH-dependent ionization. *J. Biochem.* **121**, 231-237.
- Lakowicz, J. R. & Maliwal, B. P. (1983). Oxygen quenching and fluorescence depolarization of tyrosine residues in proteins. *J. Biol. Chem.* **258**, 4794-4801.
- Larson, J. L., Ko, E. & Miranker, A. D. (2000). Direct measurement of islet amyloid polypeptide fibrillogenesis by mass spectrometry. *Protein Sci.* **9**, 427-431.
- Kudva, Y. C., Mueske, C., Butler, P. C. & Eberhardt, N. L. (1998). A novel assay in vitro of human islet amyloid polypeptide amyloidogenesis and effects of insulin secretory vesicle peptides on amyloid formation. *Biochem. J.* **331**, 809-813.
- Goldsbury, C. S., Cooper, G. J. S., Goldie, K. N., Muller, S. A., Saafi, E. L. & Gruijters, W. T. M. *et al.* (1997). Polymorphic fibrillar assembly of human amylin. *J. Struct. Biol.* **119**, 17-27.
- Cantor, C. R. & Schimmel, P. R. (1980). *Biophysical Chemistry Part II: Techniques for the Study of Biological Structure and Function*, W. H. Freeman and Company, New York.
- Jimenez, J. L., Guijarro, J. I., Orlova, E., Zurdo, J., Dobson, C. M. & Sunde, M. *et al.* (1999). Cryo-electron microscopy structure of an SH3 amyloid fibril and model of the molecular packing. *EMBO J.* **18**, 815-821.
- Balbach, J. J., Ishii, Y., Antzutkin, O. N., Leapman, R. D., Rizzo, N. W. & Dyda, F., *et al.* (2000). Amyloid fibril formation by A β ₁₆₋₂₂, a seven-residue fragment of the Alzheimer's beta-amyloid peptide, and structural characterization by solid state NMR. *Biochemistry*, **39**, 13748-13759.

30. Burkoth, T. S., Benzinger, T. L. S., Urban, V., Morgan, D. M., Gregory, D. M. & Thiyagarajan, P., *et al.* (2000). Structure of the β -amyloid₁₀₋₃₅ fibril. *JACS*, **122**, 7883-7889.
31. Horwitz, J., Strickland, E. H. & Billups, C. (1970). Analysis of the vibrational structure in the near-ultraviolet circular dichroism and absorption spectra of tyrosine derivatives and ribonuclease-A at 77 degrees K. *JACS*, **92**, 2119-2129.
32. Kaye, R., Bernhagen, J., Greenfield, N., Sweimeh, K., Brunner, H. & Voelter, W. *et al.* (1999). Conformational transitions of islet amyloid polypeptide (IAPP) in amyloid formation *in vitro*. *J. Mol. Biol.* **287**, 781-796.
33. Flory, P. J. (1969). *Statistical Mechanics of Chain Molecules*, Wiley, New York.
34. Huang, T. H., Yang, D. S., Fraser, P. E. & Chakrabarty, A. (2000). Alternate aggregation pathways of the Alzheimer beta-amyloid peptide: an *in vitro* model of preamyloid. *J. Biol. Chem.* **275**, 36436-36440.
35. Lomakin, A., Chung, D. S., Benedek, G. B., Kirschner, D. A. & Teplow, D. B. (1996). On the nucleation and growth of amyloid beta-protein fibrils: detection of nuclei and quantitation of rate constants. *Proc. Natl Acad. Sci. USA*, **93**, 1125-1129.
36. Rhoades, E., Agarwal, J. & Gafni, A. (2000). Aggregation of an amyloidogenic fragment of human islet amyloid polypeptide. *Biochim. Biophys. Acta*, **1476**, 230-238.
37. Glenner, G. G., Eanes, E. D. & Wiley, C. A. (1988). Amyloid fibrils formed from a segment of the pancreatic islet amyloid protein. *Biochem. Biophys. Res. Commun.* **155**, 608-614.
38. Tenidis, K., Waldner, M., Bernhagen, J., Fischle, W., Bergmann, M. & Weber, M., *et al.* (2000). Identification of a penta and hexapeptide of islet amyloid polypeptide (IAPP) with amyloidogenic and cytotoxic properties. *J. Mol. Biol.* **295**, 1055-1071.
39. Dobson, C. M. (1999). Protein misfolding, evolution and disease. *Trends Biochem. Sci.* **24**, 329-332.
40. Gill, S. C. & von Hippel, P. H. (1989). Calculation of protein extinction coefficients from amino acid sequence data. *Anal. Biochem.* **182**, 319-326.
41. Appel, R. D., Bairoch, A. & Hochstrasser, D. F. (1994). A new generation of information retrieval tools for biologists: the example of the ExPASy WWW server. *Trends Biochem. Sci.* **19**, 258-260.
42. Gryczynski, I., Kawski, A., Darlak, K. & Grzonka, Z. (1985). Intramolecular electronic excitation-energy transfer in dermorphine and its analogs. *J. Photochem.* **30**, 371-377.
43. Cantor, C. R. & Schimmel, P. R. (1980). *Biophysical Chemistry Part III: The Behavior of Biological Macromolecules*, W. H. Freeman and Company, New York.
44. Wolfram, Research Inc. (1996). *Mathematica*, Wolfram Research, Inc., Champaign, Illinois.

Edited by F. Cohen

(Received 11 September 2000; received in revised form 5 January 2001; accepted 28 February 2001)